CrossMark

ORIGINAL ARTICLE

Time dependence of Poisson's effect in wood IV: influence of grain angle

Ken Kawahara[1] · Kosei Ando[1] · Yusuke Taniguchi[2]

Abstract Off-axis tensile creep tests were conducted on woods taken from Japanese cypress and Kalopanax by changing the angle of load to the grain direction in the longitudinal–tangential (LT) plane. The dependence of the Poisson's ratio and trend of the viscoelastic Poisson's ratio on grain angle were investigated. The Poisson's ratios were found to reach their extrema when the grain angle was around 30°. Moreover, the Poisson's ratio in the LT plane was observed to be negative when the grain angle was in the range of 15°–45°. Comparing the experimental results with theoretical values obtained from the theory of orthotropic elasticity, it was revealed that, although the Poisson's ratio reached an extremum in both cases, the specific values did not match, especially when the angle was between 15° and 45°. Furthermore, the temporal variation of the viscoelastic Poisson's ratio was found to depend on the grain angle and the measurement plane. It also appeared to be affected by the Poisson's ratio, showing an increasing tendency above a specific Poisson's ratio (Japanese cypress: 0.196, Kalopanax: 0.102) and a decreasing tendency below it, regardless of the grain angle and measurement plane. Additionally, the increment in the viscoelastic Poisson's ratio after 24 h of creep was observed to reach its extremum when the grain angle was around 30°. Finally, by improving the six-element Frandsen–Muszynski viscoelastic model, which simultaneously considers the longitudinal and transverse strains, an eight-element model was presented, and the trend of the viscoelastic Poisson's ratio was well reproduced by this model.

Introduction

Wood is a material that has been used for building structures since ancient times. Despite the importance of studying its mechanical behavior, many aspects are still poorly understood. One of the main characteristics of the mechanical behavior of wood is anisotropy; wood is known to be an orthotropic material, and its strength varies significantly with cellular orientation and arrangement. The strength in the longitudinal (L) direction of the grain is dominantly high, followed by that in the radial (R) direction, and then by that in the tangential (T) direction. Although there have been many studies on anisotropy in directions other than the three principal axes (axes of symmetry), almost all of them consider only the Young's modulus, shear modulus, and strength. For instance, Hearmon [1] investigated the variation in Young's modulus and shear modulus with respect to the grain angle in spruce. Kollmann [2] determined the elements of the elastic compliance matrix, i.e., Young's moduli and shear moduli in the three principal stress directions, for 17 wood species. Moreover, he used Hankinson's equation [3] to study the variation in tensile strength with grain angle for white fir and basswood.

In comparison, there have been relatively few researches into the anisotropy of the Poisson's ratio of wood [4–17]. The Poisson's ratios in the direction of the principal axes of wood are defined as follows:

✉ Kosei Ando
  musica@agr.nagoya-u.ac.jp

[1] Graduate School of Bioagricultural Sciences, Nagoya University, Chikusa-ku, Nagoya 464-8601, Japan

[2] Building Products Headquarters, Daiken Corporation, 1-1 Inami, Nanto, Toyama 932-0298, Japan

$$v_{ij} = -\frac{\varepsilon_j}{\varepsilon_i} \quad (i,j = \text{L, T, R}), \qquad (1)$$

where ε_i is the longitudinal strain, ε_j is the transverse strain, and the subscripts i and j denote the directions along the three principal axes. Because of the lack of definite relationships between the Poisson's ratios and other elastic constants, density, or strength [18] and our limited understanding of how Poisson's ratio varies in different directions, many aspects of the formation mechanism of Poisson's ratio in wood remain unclear. Similar to the Young's modulus and shear modulus, the Poisson's ratio is an independent elastic constant that has significant influence on the stress–strain relationship of a material, especially under combined stresses. With increasingly complex and diversified structures being developed using wood, it is important to elucidate the formation mechanism for the anisotropy of its Poisson's effect, on which several studies have been conducted. Yamai [4] derived the Poisson's ratios for nine wood species in the directions along the grain and perpendicular to the grain through compression tests, and he found that the Poisson's ratio is not related to the specific gravity. Moreover, he theoretically investigated the dependence of Poisson's ratio on grain angle by applying the theory of orthotropic elasticity to experimental data and showed that the Poisson's ratio may be negative at some inclination angles. Although the Poisson's ratio of isotropic materials is generally positive, it has been pointed out that porous materials can have negative Poisson's ratios [19]. Sliker et al. [7] investigated the dependence of the Poisson's ratios in the LT and LR planes on grain angle in 18 hardwood species through tensile tests. They reported that the rate of change of Poisson's ratio with the angle of load to the L direction was greater in the LT plane than in the LR plane. In the LT plane, the Poisson's ratios of some wood species were negative at 20° grain angle (this supports the theory of orthotropic elasticity), and the grain angle corresponding to the minimum value differed by species. On the other hand, in the LR plane, all the wood species had non-negative Poisson's ratios regardless of the grain angle. Bukur et al. [20] and Murata et al. [13] also recorded negative Poisson's ratios in experimental data of woods. Since then, research into the dependence of the Poisson's ratio of wood on the grain angle, annual-ring angle, or microfibril angle has included several experimental and theoretical studies, which have reported extreme values at inclination angles of 20°–45° [8–13]. However, there has also been a report of a different tendency observed in the Poisson's ratio of a tropical wood, which decreases with increasing grain angle without reaching an extremum [14]. It could not be explained why this tendency differs.

In addition to anisotropy, another important characteristic of the mechanical behavior of wood is its viscoelastic property. Therefore, to grasp the mechanical response of wood under long-term loading, the time dependence of Poisson's effect must be analyzed. As Poisson's ratio is an elastic constant, it does not change with time; the parameter that characterizes the time-dependent Poisson's effect is called the viscoelastic Poisson's ratio. There have been several studies on the viscoelastic Poisson's ratio of wood in the directions of the principal axes [21–30]. Taniguchi et al. [27] conducted tensile creep tests on 12 wood species to measure $v_{LR}(t)$ and $v_{LT}(t)$ and experimentally verified that both increase with time t. As in the case of the longitudinal strain, the transverse strain during creep can be decomposed into three components, namely instantaneous strain, delayed elastic strain, and permanent strain. Taniguchi et al. also verified that the main cause for the increase in viscoelastic Poisson's ratio during creep is the considerable increase in the permanent transverse strain. Moreover, Taniguchi et al. [26] and Ando et al. [29] conducted tensile creep tests on Japanese cypress in the direction of the three principal axes and measured the transition of the six viscoelastic Poisson's ratios [$v_{LR}(t)$, $v_{LT}(t)$, $v_{RL}(t)$, $v_{RT}(t)$, $v_{TL}(t)$, and $v_{TR}(t)$]. Their results revealed that all the viscoelastic Poisson's ratios increase logarithmically with creep time and that the viscoelastic compliance matrix is non-symmetric, unlike the symmetric elastic compliance matrix. Ozyhar et al. [30] performed tensile and compressive creep tests on beech wood and reported that the six viscoelastic Poisson's ratios increased in tension and decreased in compression and that the viscoelastic compliance matrix was non-symmetric, confirming the results of Ando et al.

When wood is used as a building material, loads can be generated in various directions with respect to the grain, not necessarily in the directions of the principal axes. Therefore, the shear forces arising in the direction of the principal axes are significant, and it is important to understand the behavior of the viscoelastic Poisson's ratio under the shearing effect. However, there has been almost no research into the variation of the viscoelastic Poisson's ratio with respect to the grain angle of wood.

In this study, 24 h off-axis tensile creep tests were conducted on the LT plane of two wood species, Japanese cypress and Kalopanax, and the dependence of the Poisson's effect on grain angle and creep time was investigated.

Materials and methods

Materials

Defect-free sections from 115-year-old Japanese cypress (*Chamaecyparis obtusa* Endl.) and 81-year-old Kalopanax

(*Kalopanax septemlobus* Koidz.) woods were chosen as test samples in this study. The specimens for the tensile creep tests were cut from a sawn board, and, by changing the loading direction in the LT plane from the L direction to the T direction, specimens of seven different grain angles were prepared (0°, 15°, 30°, 45°, 60°, 75°, and 90°), as illustrated in Fig. 1. The angles 0° and 90° correspond to the L direction and T direction, respectively, and the R direction is always perpendicular to the direction of loading. The dimensions of the specimens were 180 × 15 × 15 mm (Fig. 2), and the grip sections of length 40 mm on both ends of the specimen were reinforced by tabs made of a hardwood.

All the specimens were conditioned to equilibrate a moisture content at a constant 25 °C and 55 % relative humidity (RH). The densities of these air-dried Japanese cypress and Kalopanax specimens were 417 ± 7 and 545 ± 7 kg/m³, respectively; their moisture contents were 9.4 ± 0.6 and 9.6 ± 0.1 %, respectively, and the widths of their annual rings were 0.84 and 1.92 mm, respectively.

Off-axis tensile creep tests

The off-axis tensile tests were performed using a universal testing machine (Shimadzu Autograph AGX-100kN). Biaxial strain gauges (gauge length: 2 mm; Tokyo Sokki Kenkyujo, FCA-2-11) were attached to the central regions of the four planes of the specimen to measure both the longitudinal and transverse strains, which were reported as the average of the values from the corresponding opposite planes. The viscoelastic Poisson's ratio on the LT plane of
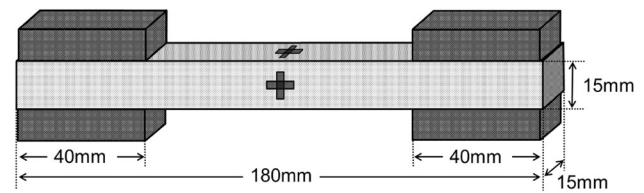
Fig. 2 Tensile test specimen. A biaxial strain gauge was attached on each of the four side planes

the specimen is denoted as $v_{LT}(\alpha, t)$ (Fig. 1), where α is the grain angle (°), and t is the creep time (h). The viscoelastic Poisson's ratio on the plane perpendicular to the LT plane, i.e., the plane whose normal direction changes from the T to L with increasing grain angle, is denoted as $v_{LR}(\alpha, t)$ (Fig. 1). Therefore, as the grain angle increases from 0° to 90°, the corresponding Poisson's ratios change from v_{LT} to v_{TL} and from v_{LR} to v_{TR}.

The tensile creep tests were conducted for 24 h. Although a 24-h period from the start is considered an early stage of creep in wood, permanent strains are generated during this period, and therefore it was assumed that the creep behaviors in this study are similar to those from long-period tests. The applied stress was 40 % of the tensile strength, which was determined in advance from static tensile tests (Table 1), and the target load was reached in 10 s. At least five samples were prepared for each grain angle, but the number of samples varied depending on the cutting procedure from one board. During the tests, the temperature and humidity were maintained at 25 °C and 55 % RH, respectively.
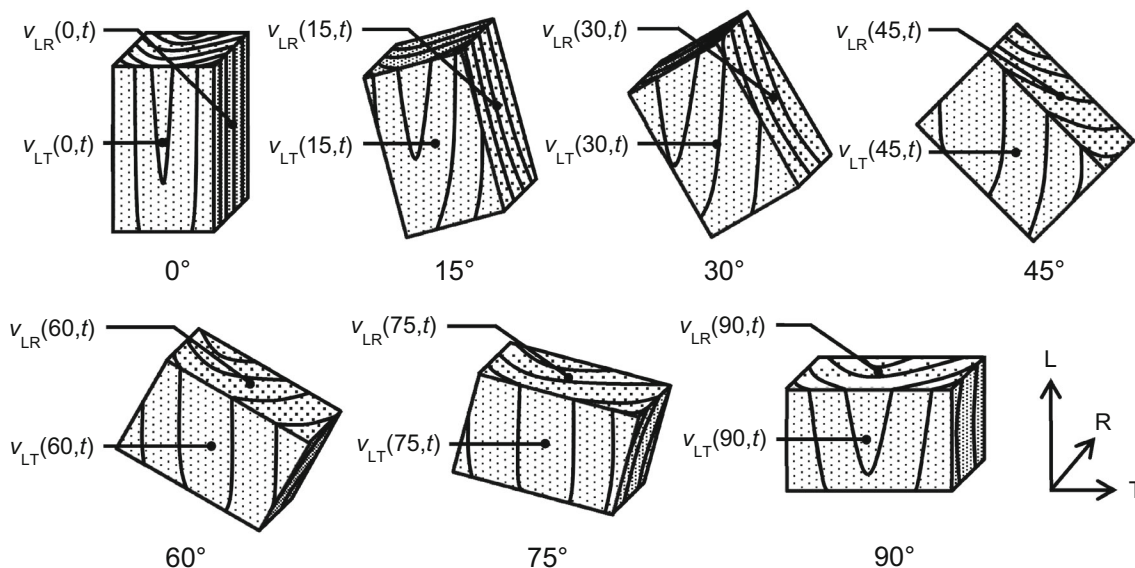
Fig. 1 Schematic of off-axis tensile specimens. $v_{LT}(\alpha, t)$ and $v_{LR}(\alpha, t)$ represent the viscoelastic Poisson's ratios. α grain angle (°), t creep time (h)

Table 1 Creep stresses and number of specimens at different grain angles

Angle (°)	Japanese cypress		Kalopanax	
	n	Creep stress (MPa)	n	Creep stress (MPa)
0	9	44.0	13	35.4
15	6	17.8	7	22.0
30	9	6.4	7	10.1
45	5	3.4	7	5.7
60	8	2.3	5	3.9
75	7	1.8	7	3.2
90	7	1.7	6	3.0

n number of specimens

Results and discussion

Young's modulus

The Young's moduli of Japanese cypress and Kalopanax obtained from the experiments at the various grain angles are presented in Fig. 3, in which the solid line represents the theoretical values calculated in accordance with Eq. (2) described later in this section. For both the wood species, the Young's modulus dropped rapidly as the grain angle first increased from 0° and then decreased gradually with further increase in the grain angle. At 0° grain angle, the Young's modulus of Japanese cypress was 10.0 GPa, and that of Kalopanax was 8.5 GPa. At 90° grain angle, the Young's modulus of Japanese cypress was 0.9 GPa, and that of Kalopanax decreased to 0.5 GPa. In the entire range, the Young's modulus of Japanese cypress was higher than that of Kalopanax at the same grain angle.

Poisson's ratio

The relationships between the grain angle and the Poisson's ratios $v_{LR}(\alpha, 0)$ and $v_{LT}(\alpha, 0)$ are shown in Figs. 4 and 5,

respectively, for both the Japanese cypress and Kalopanax. The Poisson's ratio was taken at creep time $t = 0$, i.e., at the start of the test, and the solid lines represent the theoretical values obtained from Eqs. (3) and (4), which are described later in this section. On both planes, the Poisson's ratio reached an extremum around a grain angle of 30°. However, the manner in which the extremum was approached differed: $v_{LR}(\alpha, 0)$ was convex upward, whereas $v_{LT}(\alpha, 0)$ was convex downward. Furthermore, $v_{LT}(\alpha, 0)$ exhibited the same tendency as the experimental results published by Sliker et al. [7], who conducted off-axis tensile tests in the LT plane on specimens of 18 hardwood species. According to their results, $v_{LT}(\alpha, 0)$ convexed downward and reached the extremum at a grain angle of 20°; whereas, in our study, it varied greatly at same grain angle within the range 15°–45°. Because of significant shearing effect along the L direction and its variation due to the inhomogeneity and mounting conditions of the tensile wood specimen, it was difficult to accurately measure the Poisson's ratio at these grain angles. Moreover, the Poisson's ratios $v_{LT}(\alpha, 0)$ of some specimens were negative in the range 15°–60°, implying that the specimen extended in the transverse direction when the tensile load was applied. This phenomenon, which is unlikely in isotropic materials, was assumed to occur because of the large shearing effect along the L direction and was investigated using the following theoretical equations that include this shearing effect.

Applying the generalized Hook's law to the orthotropic specimen with grain angle α, the following equations are obtained [31, 32]:

$$\frac{1}{E_{(\alpha)}} = \frac{1}{E_L}\cos^4\alpha + \left(-2\frac{v_{LT}}{E_L} + \frac{1}{G_{LT}}\right)\sin^2\alpha\cos^2\alpha + \frac{1}{E_T}\sin^4\alpha \tag{2}$$

$$v_{LR}(\alpha, 0) = E_{(\alpha)}\left(\frac{v_{LR}}{E_L}\cos^2\alpha + \frac{v_{TR}}{E_T}\sin^2\alpha\right) \tag{3}$$

Fig. 3 Young's modulus $E_{(\alpha)}$ as a function of the grain angle. The *solid line* represents a fit according to the theory of orthotropic elasticity used to estimate the shear modulus G_{LT} (Eq. 2). *Error bar* standard deviation
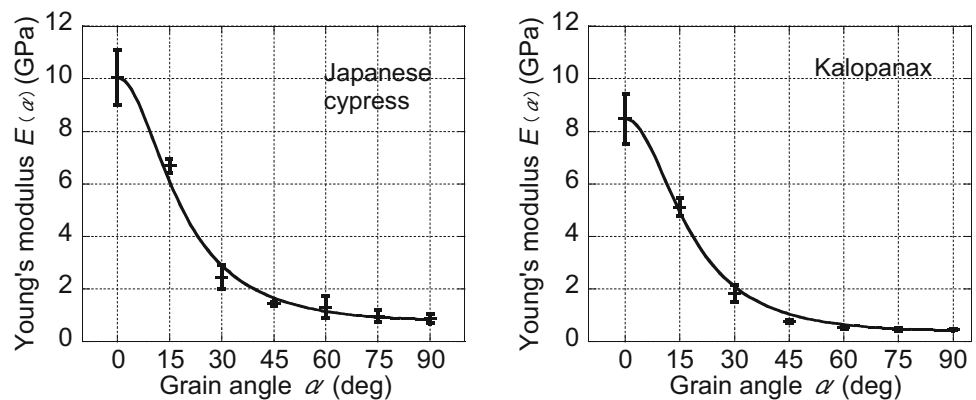
Fig. 4 Poisson's ratio $v_{LR}(\alpha, 0)$ as a function of the grain angle. The *solid line* represents a fit according to the theory of orthotropic elasticity (Eq. 3). *Error bar* standard deviation
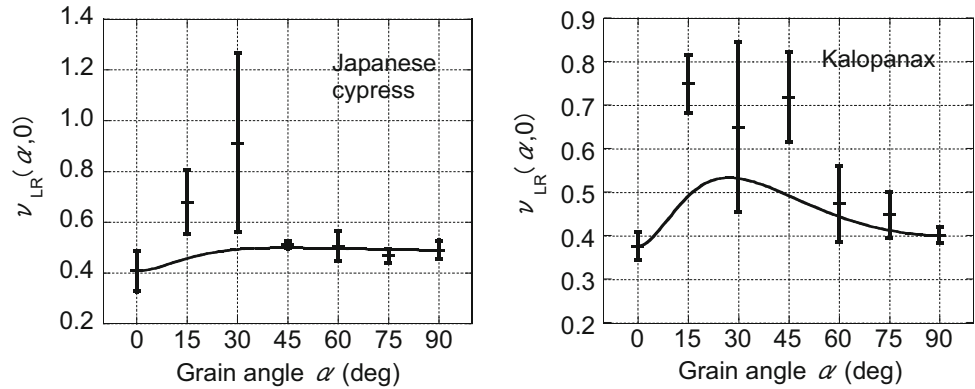
Fig. 5 Poisson's ratio $v_{LT}(\alpha, 0)$ as a function of the grain angle. The *solid line* represents a fit according to the theory of orthotropic elasticity (Eq. 4). *Error bar* standard deviation
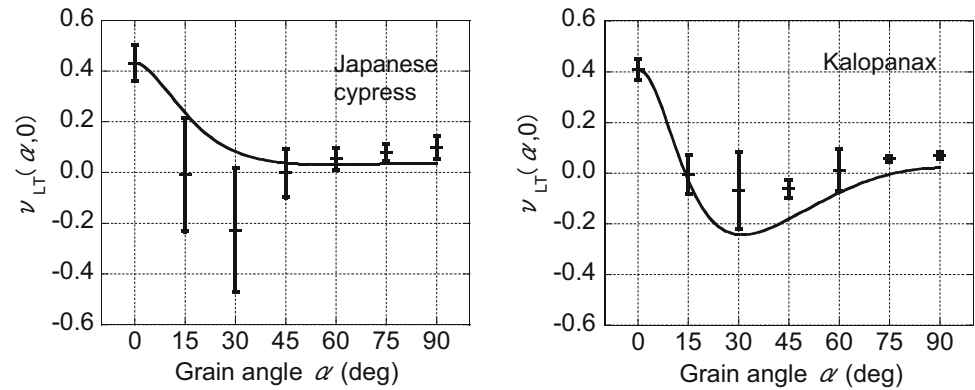
$$v_{LT}(\alpha, 0) = -E_{(\alpha)} \left\{ \left(\frac{1}{E_L} + \frac{1}{E_T} \right) \sin^2 \alpha \cos^2 \alpha - \frac{v_{LT}}{E_L} (\cos^4 \alpha + \sin^4 \alpha) - \frac{1}{G_{LT}} \sin^2 \alpha \cos^2 \alpha \right\} \tag{4}$$

in which $E_{(\alpha)}$ is the Young's modulus in the direction along the grain angle α, E_L is the Young's modulus in the L direction, E_T is the Young's modulus in the T direction, and G_{LT} is the shear modulus in the LT plane. The theoretical values of the Poisson's ratios $v_{LR}(\alpha, 0)$ and $v_{LT}(\alpha, 0)$ were calculated from Eqs. (3) and (4), respectively, using the elastic parameters tabulated in Table 2. The values of E_L, E_T, v_{LT}, v_{LR}, and v_{TR} used were taken from experimental measurements. Moreover, G_{LT} was obtained by using Eq. (2) and applying the least-squares regression method so that the sum of the squared differences was minimized between the experimental measurements of $E_{(\alpha)}$ for different grain angles and the corresponding values of $E_{(\alpha)}$ calculated using the estimated G_{LT} (and the

experimental values of E_L, E_T, and v_{LT}). The regression results are shown in Fig. 3 as a solid line, and it can be seen that they roughly match with the experimental measurements. The estimated G_{LT} was 0.804 GPa for Japanese cypress and 0.644 GPa for Kalopanax.

The theoretical values of the Poisson's ratios $v_{LR}(\alpha, 0)$ and $v_{LT}(\alpha, 0)$ at various grain angles are presented as solid lines in Figs. 4 and 5, respectively. At grain angles between 15° and 75° for Kalopanax, negative values were obtained for $v_{LT}(\alpha, 0)$, implying that a shearing effect occurs in the L direction. On the other hand, the theoretical $v_{LT}(\alpha, 0)$ for Japanese cypress did not show negative values even though some of the corresponding experimental values were negative. This difference between the two wood species is most likely due to the sensitivity of the analytical values from Eq. (4) to the estimated G_{LT} values. For both wood species, $v_{LR}(\alpha, 0)$ was convex upward, $v_{LT}(\alpha, 0)$ was convex downward, and the measured and theoretical results were consistent in the manner of the Poisson's ratios reaching their respective extrema. However, the values

Table 2 Elastic parameters used in the calculations of Eqs. (2), (3), and (4)

Species	E_L (GPa)	v_{LT}	v_{LR}	v_{TR}	E_T (GPa)	G_{LT} (GPa)
Japanese cypress	10.05	0.432	0.408	0.491	0.877	0.804
Kalopanax	8.48	0.409	0.377	0.403	0.452	0.644

itself were not well matched, especially between 15° and 45°. Two reasons were considered to explain the noticeable discrepancies between the measured and theoretical results, especially at grain angles in the range of 15°–45°. The first reason is that Eqs. (3) and (4), which were used to calculate the theoretical values, are two-dimensional (2D) equations, and therefore cannot fully express the three-dimensional phenomena, i.e., the effects from the vertical plane. The second reason is that variations in the influence of the shear forces on the L direction arise because of the inhomogeneity and mounting conditions of the wood specimens, especially at grain angles in the range of 15°–45°.

Viscoelastic Poisson's ratio

Typical cases of the evolution of the viscoelastic Poisson's ratios $v_{LR}(\alpha, t)$ and $v_{LT}(\alpha, t)$, obtained from the 24 h creep tests on Japanese cypress and Kalopanax specimens, are plotted for the various grain angles in Figs. 6 and 7, respectively. In these figures, the solid lines represent Japanese cypress, and the dotted lines represent Kalopanax. In all cases, the viscoelastic Poisson's ratios first underwent rapid change once creep started, and then showed more gradual change over time. For both wood species, $v_{LR}(\alpha, t)$ increased regardless of the grain angle; whereas $v_{LT}(\alpha, t)$ increased at the grain angle of 0°, increased or decreased at the grain angle of 15°, and decreased at the grain angles equal to or greater than 30°. However, the results shown in Figs. 6 and 7 are only from one set of specimens, and thus it cannot be concluded that all specimens at a certain grain angle will show the same trend. For example, although the $v_{LT}(15, t)$ of the Kalopanax specimen presented in Fig. 7 increased, there were specimens that showed a decrease in the $v_{LT}(15, t)$.

Therefore, to express the creep test results quantitatively with respect to grain angle, the increments in the viscoelastic Poisson's ratios after 24 h of creep will be examined next.

The increment in the viscoelastic Poisson's ratio with creep time t (h) is defined by the following equation:

$$\Psi_{Li}(\alpha, t) = v_{Li}(\alpha, t) - v_{Li}(\alpha, 0) \quad (i = R, T) \tag{5}$$

The increments in the viscoelastic Poisson's ratios after 24 h of creep, $\Psi_{LR}(\alpha, 24)$ and $\Psi_{LT}(\alpha, 24)$, are plotted against the grain angle in Figs. 8 and 9, respectively. Both quantities approached the extrema around a grain angle of 30° in the two wood species, but $\Psi_{LR}(\alpha, 24)$ was convex upward; whereas $\Psi_{LT}(\alpha, 24)$ was convex downward. These trends are similar to the dependence of the Poisson's ratios on grain angle previously shown in Figs. 4 and 5. Without taking into account the grain angle and measurement plane, the relationship between the Poisson's ratio and the increment in the viscoelastic Poisson's ratio at $t = 24$ h is presented in Fig. 10 for the two wood species. According to the results of linear regression, these two parameters are positively correlated with a 1 % significance level. The regression results also suggested that there exists a Poisson's ratio (denoted as v_0) at zero increment of viscoelastic Poisson's ratio. From the regression equation, the values of this Poisson's ratio were obtained as $v_0 = 0.196$ for Japanese cypress and $v_0 = 0.102$ for Kalopanax. Regardless of the grain angle and measurement plane, the viscoelastic Poisson's ratio showed an increasing tendency at Poisson's ratios above v_0 and a decreasing tendency at Poisson's ratios below v_0, i.e., the influence of the Poisson's ratio on the trend of the viscoelastic Poisson's ratio was evident.
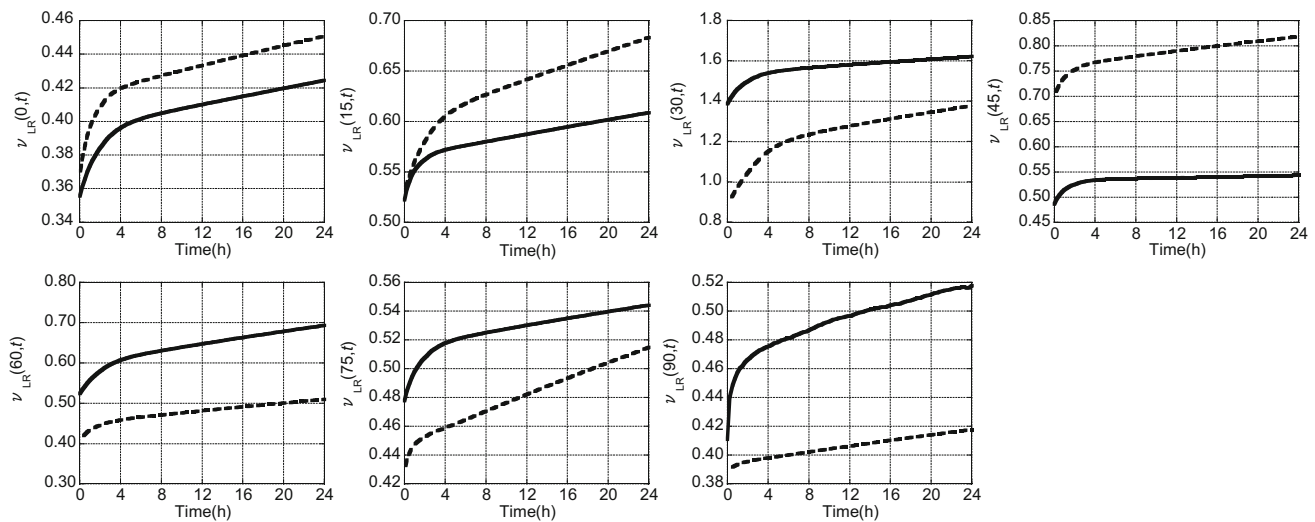
Fig. 6 Typical progression of viscoelastic Poisson's ratio $v_{LR}(\alpha, t)$ measured during creep. *Solid line* Japanese cypress, *dotted line* Kalopanax
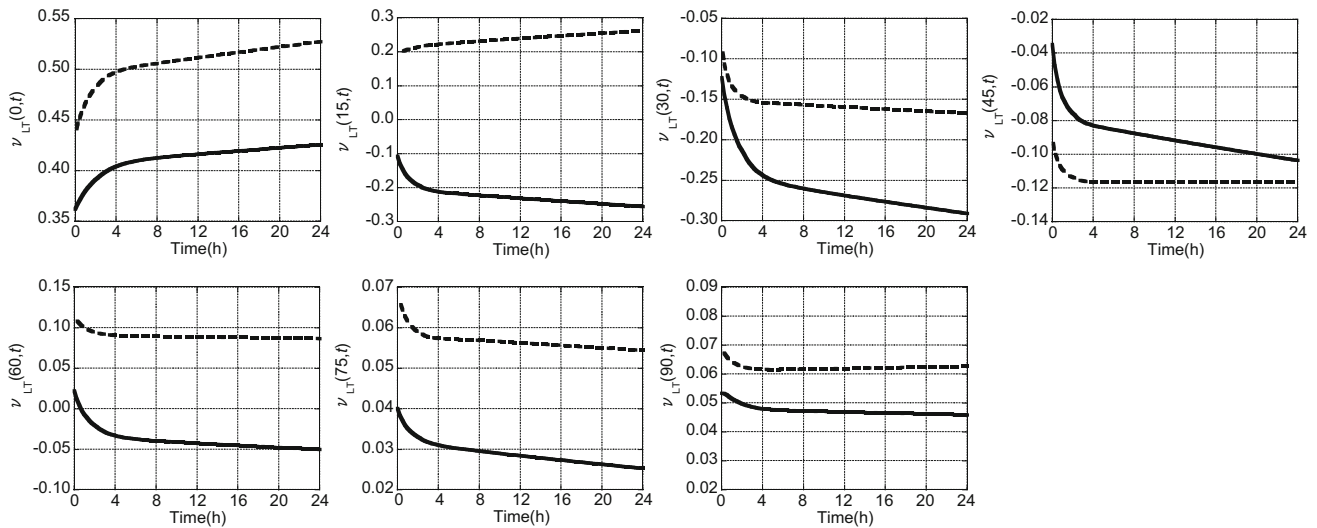
Fig. 7 Typical progression of viscoelastic Poisson's ratio $v_{LT}(\alpha, t)$ measured during creep. *Solid line* Japanese cypress, *dotted line* Kalopanax

Fig. 8 Increment in viscoelastic Poisson's ratio after 24 h of creep, $\Psi_{LR}(\alpha, 24)$, as a function of the grain angle. *Error bar* standard deviation
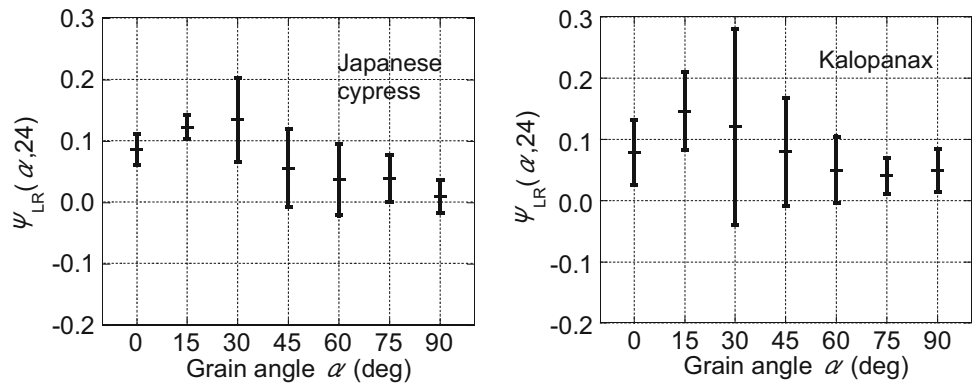
Fig. 9 Increment in viscoelastic Poisson's ratio after 24 h of creep, $\Psi_{LT}(\alpha, 24)$, as a function of the grain angle. *Error bar* standard deviation
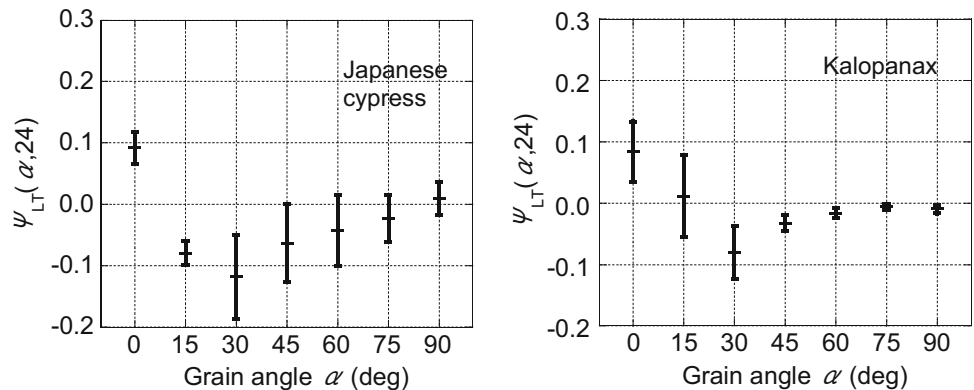
Estimation of viscoelastic Poisson's ratio using a 2D viscoelasticity model

To express the 2D viscoelasticity of wood, Frandsen et al. [25] proposed a six-element model (Frandsen–Muszynski model) that included the components of instantaneous strain and delayed elastic strain in both the longitudinal and transverse directions. In this study, their model was improved by adding the permanent strain components, and thus an eight-element 2D creep model was obtained, as illustrated in Fig. 11 (longitudinal strain direction: L, transverse strain direction: R). It can be confirmed

Fig. 10 Relationship between Poisson's ratio $v_{Li}(\alpha, 0)$ and increment in viscoelastic Poisson's ratio after 24 h of creep, $\Psi_{Li}(\alpha, 24)$. $i = $ R or T. *Double asterisk* significant at $p < 0.01$
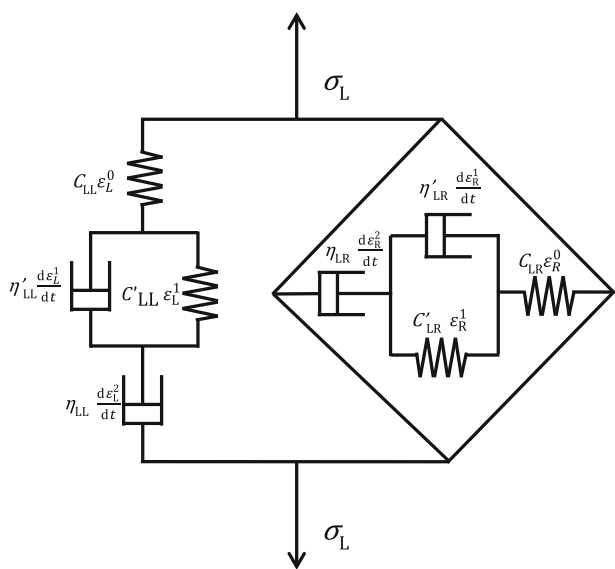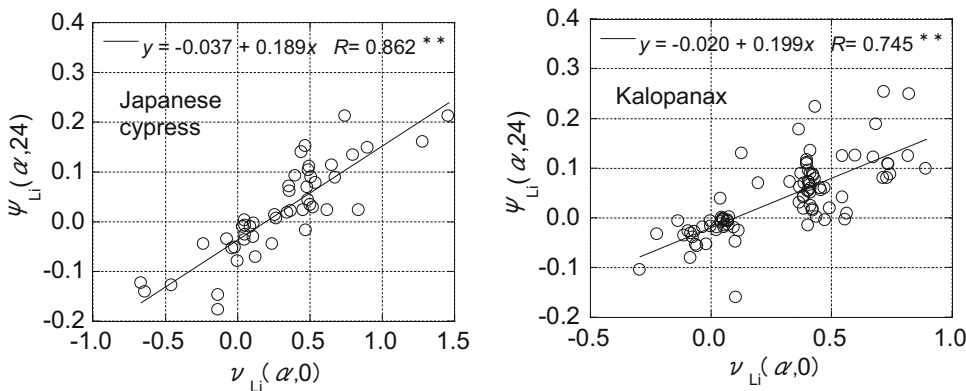
Fig. 11 2D viscoelastic model considering Poisson's effect (modified Frandsen–Muszynski model) under uniaxial creep stress in L direction, σ_L

experimentally that the transverse strain in wood undergoing creep also consists of instantaneous strain, delayed elastic strain, and permanent strain [27], similar to the longitudinal strain. Therefore, the proposed model that considers these three strain components is appropriate. In Fig. 11, the section on the left represents the longitudinal strain, and the section on the right represents the transverse strain resulting from Poisson's effect. Each of them is represented by a series arrangement of a spring, Kelvin–Voigt element, and dashpot. C and C' denote the stiffness moduli of the springs; η and η' denote the viscosity coefficients of the dashpots. The total longitudinal strain in the L direction, ε_L, is expressed as the sum of the instantaneous strain in the spring, ε_L^0, the delayed elastic strain in the Kelvin–Voigt element, ε_L^1, and the permanent strain in the dashpot, ε_L^2, yielding the following equation:

$$\varepsilon_L = \varepsilon_L^0 + \varepsilon_L^1 + \varepsilon_L^2 \tag{6}$$

Similarly, the total transverse strain in the R direction, ε_R, can be defined as the sum of the instantaneous strain ε_R^0, the delayed elastic strain ε_R^1, and the permanent strain ε_R^2, yielding the following equation:

$$\varepsilon_R = \varepsilon_R^0 + \varepsilon_R^1 + \varepsilon_R^2 \tag{7}$$

For the instantaneous strain, delayed elastic strain, and permanent strain components, the relationship between the stress in the L direction, σ_L, and the respective strain can be written as follows (Fig. 11):

$$\sigma_L = C_{LL}\varepsilon_L^0 + C_{LR}\varepsilon_R^0 \tag{8}$$

$$\sigma_L = C'_{LL}\varepsilon_L^1 + \eta'_{LL}\frac{d\varepsilon_L^1}{dt} + C'_{LR}\varepsilon_R^1 + \eta'_{LR}\frac{d\varepsilon_R^1}{dt} \tag{9}$$

$$\sigma_L = \eta_{LL}\frac{d\varepsilon_L^2}{dt} + \eta_{LR}\frac{d\varepsilon_R^2}{dt} \tag{10}$$

The stress in the R direction, σ_R, can be expressed in a similar manner. For each of the three strain components (i–iii), matrix notation can be used to obtain the following:

(i) instantaneous strain

$$\begin{pmatrix} \sigma_L \\ \sigma_R \end{pmatrix} = \begin{pmatrix} C_{LL} & C_{LR} \\ C_{RL} & C_{RR} \end{pmatrix} \begin{pmatrix} \varepsilon_L^0 \\ \varepsilon_R^0 \end{pmatrix} \tag{11}$$

or

$$\begin{pmatrix} \varepsilon_L^0 \\ \varepsilon_R^0 \end{pmatrix} = \begin{pmatrix} C_{LL} & C_{LR} \\ C_{RL} & C_{RR} \end{pmatrix}^{-1} \begin{pmatrix} \sigma_L \\ \sigma_R \end{pmatrix} \tag{12}$$

(ii) delayed elastic strain

$$\begin{pmatrix} \sigma_L \\ \sigma_R \end{pmatrix} = \begin{pmatrix} C'_{LL} & C'_{LR} \\ C'_{RL} & C'_{RR} \end{pmatrix} \begin{pmatrix} \varepsilon_L^1 \\ \varepsilon_R^1 \end{pmatrix} + \begin{pmatrix} \eta'_{LL} & \eta'_{LR} \\ \eta'_{RL} & \eta'_{RR} \end{pmatrix} \begin{pmatrix} \frac{d\varepsilon_L^1}{dt} \\ \frac{d\varepsilon_R^1}{dt} \end{pmatrix} \tag{13}$$

Rearranging gives:

$$\begin{pmatrix} \dfrac{d\varepsilon_L^1}{dt} \\ \dfrac{d\varepsilon_R^1}{dt} \end{pmatrix} = \begin{pmatrix} \eta'_{LL} & \eta'_{LR} \\ \eta'_{RL} & \eta'_{RR} \end{pmatrix}^{-1} \begin{pmatrix} \sigma_L \\ \sigma_R \end{pmatrix}$$
$$\quad - \begin{pmatrix} \eta'_{LL} & \eta'_{LR} \\ \eta'_{RL} & \eta'_{RR} \end{pmatrix}^{-1} \begin{pmatrix} C'_{LL} & C'_{LR} \\ C'_{RL} & C'_{RR} \end{pmatrix} \begin{pmatrix} \varepsilon_L^1 \\ \varepsilon_R^1 \end{pmatrix} \tag{14}$$

In uniaxial creep tests, $\sigma_R = 0$. After simple replacement, the equation above can be summarized as follows:

$$\begin{pmatrix} \eta'_{LL} & \eta'_{LR} \\ \eta'_{RL} & \eta'_{RR} \end{pmatrix}^{-1} = \begin{pmatrix} a & b \\ c & d \end{pmatrix} \tag{15}$$

$$\begin{pmatrix} \eta'_{LL} & \eta'_{LR} \\ \eta'_{RL} & \eta'_{RR} \end{pmatrix}^{-1} \begin{pmatrix} C'_{LL} & C'_{LR} \\ C'_{RL} & C'_{RR} \end{pmatrix} = \begin{pmatrix} e & f \\ g & h \end{pmatrix} \tag{16}$$

$$\frac{d\varepsilon_L^1}{dt} = a\sigma_L - \left(e\varepsilon_L^1 + f\varepsilon_R^1\right) \tag{17}$$

$$\frac{d\varepsilon_R^1}{dt} = c\sigma_L - \left(g\varepsilon_L^1 + h\varepsilon_R^1\right) \tag{18}$$

Equation (17) can be re-arranged into as

$$\varepsilon_R^1 = -\frac{1}{f}\frac{d\varepsilon_L^1}{dt} - \frac{e}{f}\varepsilon_L^1 + \frac{a}{f}\sigma_L \tag{19}$$

Differentiating Eq. (19) with respect to time t yields

$$\frac{d\varepsilon_R^1}{dt} = -\frac{1}{f}\frac{d^2\varepsilon_L^1}{dt^2} - \frac{e}{f}\frac{d\varepsilon_L^1}{dt} \tag{20}$$

Substituting Eqs. (19) and (20) into Eq. (18) and rearranging,

$$\frac{d^2\varepsilon_L^1}{dt^2} + \frac{d\varepsilon_L^1}{dt}(e+h) + \varepsilon_L^1(eh - fg) = \sigma_L(ah - fc) \tag{21}$$

After simple replacement, Eq. (21) becomes

$$e + h = 2p, \quad eh - fg = q, \quad \sigma_L(ah - fc) = r \tag{22}$$

$$\frac{d^2\varepsilon_L^1}{dt^2} + \frac{d\varepsilon_L^1}{dt}2p + \varepsilon_L^1 q = r \tag{23}$$

Solving the differential Eq. (23) with the initial condition $\varepsilon_L^1 = 0$ at $t = 0$ gives

$$\varepsilon_L^1 = C_1\left(e^{\lambda_1 t} - 1\right) + C_2\left(e^{\lambda_2 t} - 1\right), \tag{24}$$

where

$$C_1 = \frac{r\left(-p - \sqrt{p^2 - q}\right) + aq\sigma_L}{2q\sqrt{p^2 - q}} \tag{25}$$

$$C_2 = -\frac{r}{q} - \frac{r\left(-p - \sqrt{p^2 - q}\right) + aq\sigma_L}{2q\sqrt{p^2 - q}} \tag{26}$$

$$\lambda_1 = \sqrt{p^2 - q} - p, \quad \lambda_2 = -\sqrt{p^2 - q} - p \tag{27}$$

Similarly, the transverse strain component ε_R^1 can be computed by the following equation:

$$\varepsilon_R^1 = C_3\left(e^{\lambda_3 t} - 1\right) + C_4\left(e^{\lambda_4 t} - 1\right) \tag{28}$$

Fig. 12 Progression of longitudinal (ε_L) and transverse (ε_R or ε_T) strains under creep load in L direction for Japanese cypress. Solid line experimental, dotted line theoretical from the model in Fig. 11
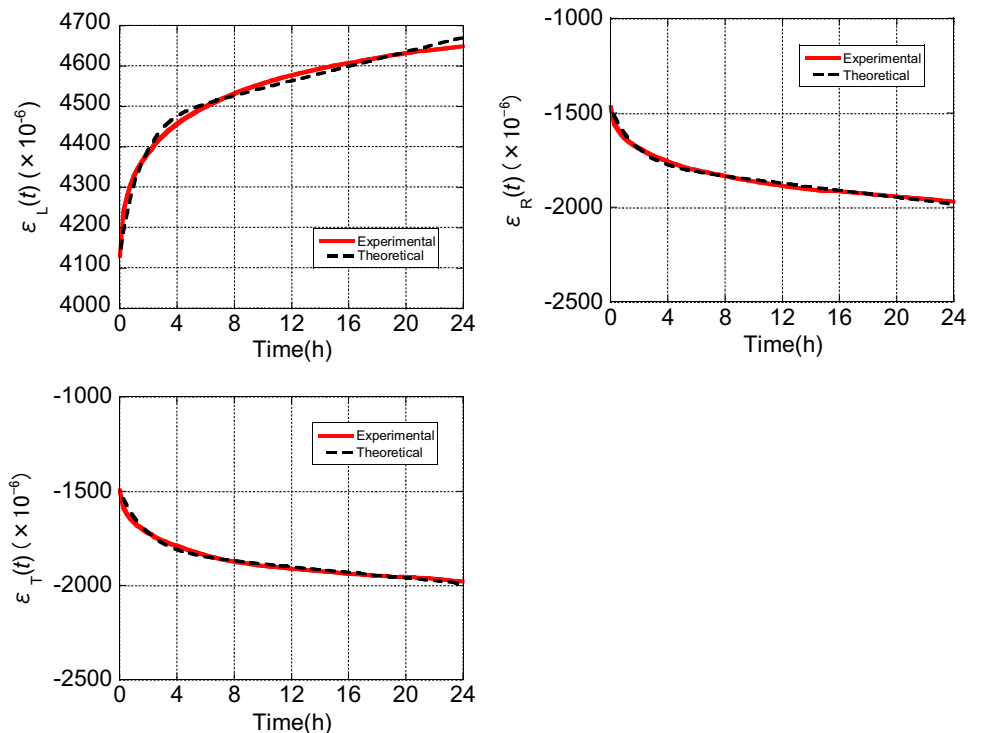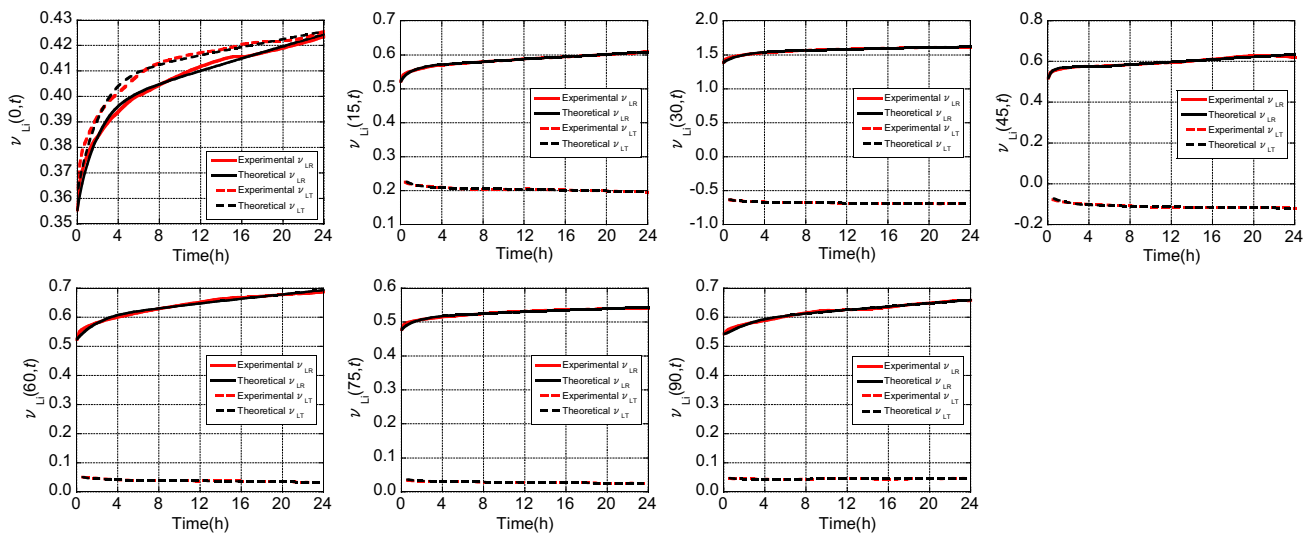
Fig. 13 Progression of viscoelastic Poisson's ratios $v_{Li}(\alpha, t)$ for Japanese cypress. $i = $ R or T. *Solid line* $v_{LR}(\alpha, t)$, *dotted line* $v_{LT}(\alpha, t)$. Theoretical values were obtained from the model in Fig. 11
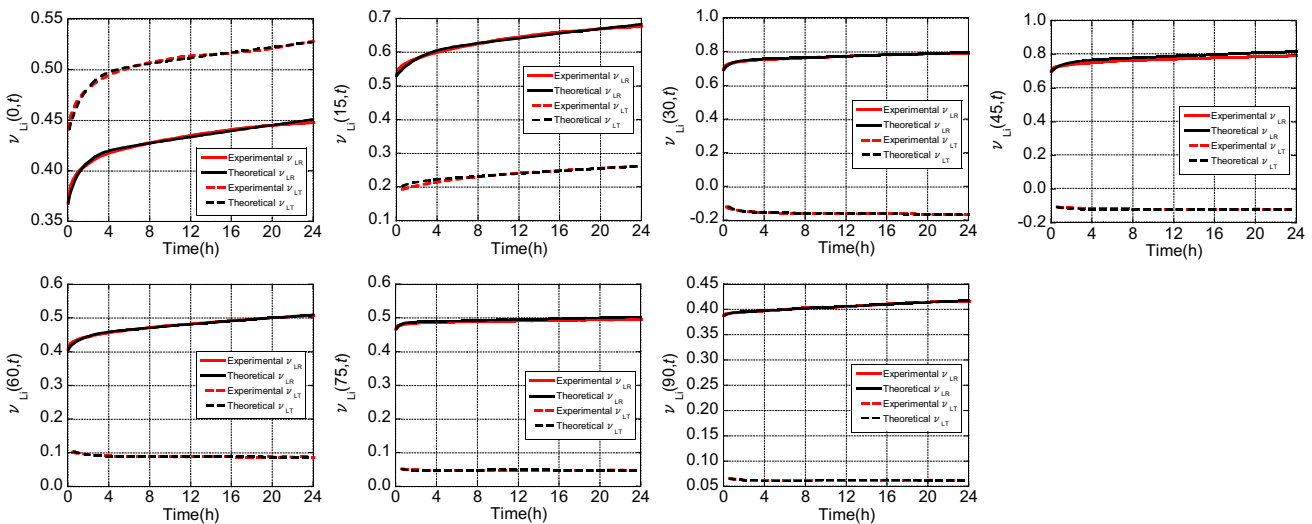
Fig. 14 Progression of viscoelastic Poisson's ratios $v_{Li}(\alpha, t)$ for Kalopanax. $i = $ R or T. *Solid line* $v_{LR}(\alpha, t)$, *Dotted line* $v_{LT}(\alpha, t)$. Theoretical values were obtained from the model in Fig. 11

(iii) permanent strain

$$\begin{pmatrix} \sigma_L \\ \sigma_R \end{pmatrix} = \begin{pmatrix} \eta_{LL} & \eta_{LR} \\ \eta_{RL} & \eta_{RR} \end{pmatrix} \begin{pmatrix} \dfrac{d\varepsilon_L^2}{dt} \\ \dfrac{d\varepsilon_R^2}{dt} \end{pmatrix} \tag{29}$$

or

$$\begin{pmatrix} \dfrac{d\varepsilon_L^2}{dt} \\ \dfrac{d\varepsilon_R^2}{dt} \end{pmatrix} = \begin{pmatrix} \eta_{LL} & \eta_{LR} \\ \eta_{RL} & \eta_{RR} \end{pmatrix}^{-1} \begin{pmatrix} \sigma_L \\ \sigma_R \end{pmatrix} \tag{30}$$

Integrating Eq. (30) with respect to time t with the initial conditions $\varepsilon_L^2 = 0$ and $\varepsilon_R^2 = 0$ at $t = 0$ yields

$$\begin{pmatrix} \varepsilon_L^2 \\ \varepsilon_R^2 \end{pmatrix} = \begin{pmatrix} \eta_{LL} & \eta_{LR} \\ \eta_{RL} & \eta_{RR} \end{pmatrix}^{-1} \begin{pmatrix} \sigma_L \\ \sigma_R \end{pmatrix} t \tag{31}$$

As can be seen, the permanent strains ε_L^2 and ε_R^2 are proportional to time t. The constants of proportionality are defined as A and B, respectively.

Thus, from (ii) and (iii), the longitudinal and transverse creep strains can be expressed as follows:

$$\varepsilon_L^1 + \varepsilon_L^2 = C_1(e^{\lambda_1 t} - 1) + C_2(e^{\lambda_2 t} - 1) + At \tag{32}$$

$$\varepsilon_R^1 + \varepsilon_R^2 = C_3(e^{\lambda_3 t} - 1) + C_4(e^{\lambda_4 t} - 1) + Bt, \tag{33}$$

where C_1, C_2, C_3, C_4, λ_1, λ_2, λ_3, λ_4, A, and B are the constants from the stiffness moduli of the springs, viscosity

coefficients of the dashpots, and stress. From Eqs. (32) and (33), the unknown quantities were calculated by performing regression analyses on the measured longitudinal and transverse strains. The progressions of the creep strains were then predicted using these equations using instantaneous strain components obtained from experimental measurements. For example, Fig. 12 shows the regression results of the strains in Japanese cypress at a grain angle of 0°, and the experimental results were found to be in good agreement with the theoretical values from the model. Moreover, the regression curve of the viscoelastic Poisson's ratio was derived from the ratio of transverse to longitudinal strains, and the results for Japanese cypress and Kalopanax are presented in Figs. 13 and 14, respectively. Again, the experimental results and theoretical values from the model were found to be in good agreement. Therefore, the eight-element creep model proposed in this study can be used to estimate the viscoelastic Poisson's ratio at any creep time t. However, this model does not currently have a practical use because many of the quantities remain unclear. Further experimental and theoretical works, to determine the unknown quantities (all stiffness moduli of the springs and all viscosity coefficients of the dashpots), are still needed to establish this model.

Conclusions

Through off-axis tensile creep tests on the LT plane of Japanese cypress and Kalopanax specimens, the dependence of the Poisson effect in wood on grain angle and creep time was investigated. The Poisson's ratios reached their extrema around a grain angle of 30°, which was considered to be caused by the influence of shear forces in the L direction of wood. Moreover, the Poisson's ratio in the LT plane was found to be negative in the range of 15°–45°. The theoretical Poisson's ratios were calculated from the theory of orthotropic elasticity, and they were similar to the experimental results in the manner of reaching the respective extrema, but the actual values differed.

The progression of the viscoelastic Poisson's ratio varied depending on the grain angle and the measurement plane, and the increment in the viscoelastic Poisson's ratio after 24 h of creep reached its extremum at a grain angle of around 30°. These trends were also presumed to be caused by the shear forces in the L direction of wood, but further research on the time dependence of the apparent shear modulus $G_{LT}(t)$ is required to understand this influence more clearly. Taking into account the Poisson effect, an eight-element viscoelastic model was presented, and the progression of viscoelastic Poisson's ratio under uniaxial creep was well reproduced by this model. However, this model does not currently have a practical use because many of the quantities remain unclear. Further experimental and theoretical works are still needed to establish this model.

References

1. Hearmon RFS (1948) The effect of grain angle. In: The elasticity of wood and plywood. Forest products research special report No.7. His Majesty's Stationery Office, London, pp 30–35
2. Kollmann FFP (1968) Mechanics and rheology of wood. Principles of wood science and technology I: solid wood. Springer, Berlin, pp 292–419
3. Hankinson RL (1921) Investigation of crushing strength of spruce at varying angles of grain. Air Serv Inf Circ 259:3–15
4. Yamai R (1957) On the orthotropic properties of wood in compression. J Jpn For Soc 39:328–338
5. Morooka T, Ohgama T, Yamada T (1979) Poisson's ratio of porous material (in Japanese). J Soc Mater Sci Jpn 28:635–640
6. Ohgama T (1982) Poisson's ratio of wood as porous material (in Japanese). Bull Fac Educ Chiba Univ Part II 31:99–107
7. Sliker A, Yu Y (1993) Elastic constants for hardwoods measured from plate and tension tests. Wood Fiber Sci 25:8–22
8. Reiterer A, Stanzl-Tschegg SE (2001) Compressive behaviour of softwood under uniaxial loading at different orientations to the grain. Mech Mater 33:705–715
9. Liu JY (2002) Analysis of off-axis tension test of wood specimens. Wood Fiber Sci 34:205–211
10. Marklund E, Varna J (2009) Modeling the effect of helical fiber structure on wood fiber composite elastic properties. Appl Compos Mater 16:245–262
11. Qing H, Mishnaevsky L Jr (2010) 3D Multiscale micromechanical model of wood: from annual rings to microfibrils. Int J Solids Struct 47:1253–1267
12. Garab J, Keunecke D, Hering S, Szalai J, Niemz P (2010) Measurement of standard and off-axis elastic moduli and Poisson's ratios of spruce and yew wood in the transverse plane. Wood Sci Technol 44:451–464
13. Murata K, Tanahashi H (2010) Measurement of Young's modulus and Poisson's ratio of wood specimens in compression test (in Japanese). J Soc Mater Sci Jpn 59:285–290
14. Mascia NT, Nicolas EA (2013) Determination of Poisson's ratios in relation to fiber angle of a tropical wood species. Constr Build Mater 41:691–696
15. Yoshihara H, Ohta M (1995) Measurement of the in-plane elastic constants of wood by the uniaxial compression test using a single specimen. Mokuzai Gakkaishi 41:218–222
16. Keunecke D, Hering S, Niemz P (2008) Three-dimensional elastic behaviour of common yew and Norway spruce. Wood Sci Technol 42:633–647
17. Jeong GY, Hindman DP (2010) Modeling differently oriented loblolly pine strands incorporating variation of intraring properties using a stochastic finite element method. Wood Fiber Sci 42:51–61
18. Bodig J, Goodman JR (1973) Prediction of elastic parameters for wood. Wood Sci 5:249–264
19. Lakes R (1987) Foam structures with a negative Poisson's ratio. Science 235:1038–1040
20. Bucur V, Najafi SK (2003) Negative Poisson ratios in wood and particleboard with ultrasonic technique. Nondestructive characterization of materials XI. Springer, Berlin, pp 47–51

21. Anderson B, Murphey WK (1970) An investigation of time-dependency of Poisson's ratio in compressively loaded wood. Res Br Sch For Resour Pa State Univ 4:39–41

22. Schniewind AP, Barrett JD (1972) Wood as a linear orthotropic viscoelastic material. Wood Sci Technol 6:43–57

23. Sobue N, Takemura T (1979) Poisson's ratios in dynamic viscoelasticity of wood as two-dimensional materials. Mokuzai Gakkaishi 25:258–263

24. Hayashi K, Felix B, Le Govic C (1993) Wood viscoelastic compliance determination with special attention to measurement problems. Mater Struct 26:370–376

25. Frandsen HL, Muszynski L (2006) Modeling of the time and strain dependent Poisson effect in wood and wood-based composites. In: Fioravanti M, Macchioni N (eds) Proceeding of the international conference on integrated approach to wood structure, behaviour and applications. Joint meeting of ESWM and COST Action E35. Florence, Italy, 15–17 May 2006, pp 139–144

26. Taniguchi Y, Ando K, Yamamoto H (2010) Determination of three-dimensional viscoelastic compliance in wood by tensile creep test. J Wood Sci 56:82–84

27. Taniguchi Y, Ando K (2010) Time dependence of Poisson's effect in wood I: the lateral strain behavior. J Wood Sci 56:100–106

28. Taniguchi Y, Ando K (2010) Time dependence of Poisson's effect in wood II: volume change during uniaxial tensile creep. J Wood Sci 56:350–354

29. Ando K, Mizutani M, Taniguchi Y, Yamamoto H (2013) Time dependence of Poisson's effect in wood III: asymmetry of three-dimensional viscoelastic compliance matrix of Japanese cypress. J Wood Sci 59:290–298

30. Ozyhar T, Hering S, Niemz P (2013) Viscoelastic characterization of wood: time dependence of the orthotropic compliance in tension and compression. J Rheol 57:699–717

31. Bodig J, Jayne BA (1982) Orthotropic elasticity. Mechanics of wood and wood composites. Van Nostrand Reinhold, New York, pp 87–126

32. Qing H, Mishnaevsky L Jr (2009) 3D hierarchical computational model of wood as a cellular material with fibril reinforced, heterogeneous multiple layers. Mech Mater 41:1034–1049